Controlled n#Doping of Naphthalene#Diimide#Based 2D Polymers

Controlled *n*-Doping of Naphthalene Diimide-Based Two-Dimensional Polymers

*Austin M. Evans, Kelsey A. Collins, Sangni Xun, Taylor G. Allen, Samik Jhulki, Ioannina Castano, Hannah L. Smith, Michael J. Strauss, Alexander K. Oanta, Lujia Liu, Lei Sun, Obadiah G. Reid, Gjergji Sini, Danilo Puggioni, James M. Rondinelli, Tijana Rajh, Nathan C. Gianneschi, Antoine Kahn, Danna E. Freedman, Hong Li, Stephen Barlow, Garry Rumbles, Jean-Luc Brédas, Seth R. Marder, William R. Dichtel**

A. M. Evans, K. A., Collins, I. Castano, M. J. Strauss, A. K. Oanta, L. Liu, N. C. Gianneschi, D. E. Freedman, W. R. Dichtel
Department of Chemistry, Northwestern University, Evanston, IL, 60208, USA
E-mail: wdichtel@northwestern.edu

S. Xun, S. Jhulki, S. Barlow, S.R. Marder
School of Chemistry and Biochemistry, Georgia Institute of Technology, Atlanta, GA, 30332, USA
Center for Organic Photonics and Electronics, Georgia Institute of Technology, Atlanta, GA, 30332, USA

S. Xun
College of Environmental Science and Engineering, Hunan University, Changsha 410082, P. R. China

T. G. Allen, O. G. Reid, G. Rumbles
Center for Chemistry and Nanoscience, National Renewable Energy Laboratory, 15013 Denver West Parkway, Golden, CO 80401, USA

H. L. Smith, A. Kahn
Department of Electrical Engineering, Princeton University, Princeton, NJ, 08544, USA

L. Sun, T. Rajh
Center for Nanoscale Materials, Argonne National Laboratory, Lemont, IL 60439, USA

O. G. Reid, G. Rumbles
Renewable and Sustainable Energy Institute, Department of Chemistry, University of Colorado Boulder, Boulder, CO 80309, USA

G. Sini, H. Li, J.-L. Brédas
Department of Chemistry and Biochemistry, The University of Arizona, Tucson, AZ 85721 USA,

G. Sini
CY Cergy Paris Université, Laboratoire de Physicochimie des Polymères et des Interfaces, EA 2528, 5 mail Gay-Lussac, Cergy-Pontoise Cedex, 95031, France.

D. Puggioni, J. R. Rondinelli, N.C. Gianneschi
Department of Materials Science and Engineering, Northwestern University, Evanston, IL 60208, USA

N.C. Gianneschi
International Institute for Nanotechnology, Department of Biomedical Engineering, Department of Pharmacology, Simpson Querrey Institute, and Chemistry of Life Processes Institute, Evanston, IL 60208, USA

Keywords: Organic semiconductor, two-dimensional polymers, *n*-type molecular doping, conductive polymers

This article has been accepted for publication and undergone full peer review but has not been through the copyediting, typesetting, pagination and proofreading process, which may lead to differences between this version and the Version of Record. Please cite this article as doi: 10.1002/adma.202101932.

Abstract

Two-dimensional polymers (2DPs) are promising as structurally well-defined, permanently porous, organic semiconductors. However, 2DPs are nearly always isolated as closed shell organic species with limited charge carriers, which leads to low bulk conductivities. Here, we enhance the bulk conductivity of two naphthalene diimide (NDI)-containing 2DP semiconductors by controllably *n*-doping the NDI units using cobaltocene ($CoCp_2$). Optical and transient microwave spectroscopy reveals that both as-prepared NDI-containing 2DPs are semiconducting with sub-2 eV optical bandgaps and photoexcited charge-carrier lifetimes of tens of nanoseconds. Following reduction with $CoCp_2$, both 2DPs largely retain their periodic structures and exhibit optical and electron-spin resonance spectroscopic features consistent with the presence of NDI-radical anions. While the native NDI-based 2DPs are electronically insulating, maximum bulk conductivities of $>10^{-4}$ *S* cm^{-1} are achieved by substoichiometric levels of *n*-doping. Density functional theory calculations show that the strongest electronic couplings in these 2DPs exist in the out-of-plane (π-stacking) crystallographic directions, which indicates that cross-plane electronic transport through NDI stacks is primarily responsible for the observed electronic conductivity. Taken together, this study underlines that controlled molecular doping is a useful approach to access structurally well-defined, paramagnetic, 2DP *n*-type semiconductors with measurable bulk electronic conductivities of interest for electronic or spintronic devices.

Manuscript

Two-dimensional polymers (2DPs) are macromolecular sheets that combine permanent porosity with long-range order.[1] This periodicity enables the deterministic placement of chemical functionality in porous organic materials. This structural regularity, in principle, can lead to tailored emergent electronic and magnetic phenomena that are of interest for electronic and spintronic devices.[1, 2, 3] For example, computational and spectroscopic investigations have exposed that long-lived charge-separated states exist in some semiconducting 2DPs.[1, 3, 4, 5] However, the experimentally measured electronic conductivities of 2DPs are low, which have historically limited fundamental investigations and the use of 2DPs in some applications. Low conductivities are expected for most high-quality 2DPs, as a low number of free charge carriers is expected in closed shell organic systems with bandgaps >1 eV. Even when free charge carriers can be deliberately introduced through doping, many 2DPs exhibit low conductivities, likely attributable to the poor conjugation afforded by many 2D polymerization chemistries and/or the high densities of trap states in defect-prone materials. Addressing the long-standing challenge of developing highly conductive 2DPs that are porous, structurally precise, organic semiconductors is of potential interest for many devices including chemical sensors,[6] optoelectronics,[7] spin-valves,[8] and thermoelectrics.[9]

Electrical doping with molecular redox agents can be used to increase conductivity by chemical oxidation (*p*-doping) or reduction (*n*-doping) both through increasing the number of charge carriers and increasing the mobility of charge carriers by filling trap states.[10, 11] Despite the development of molecular doping techniques for organic molecules and linear polymers, doping of 2DPs has not been extensively investigated.[11, 12, 13] Currently, experimental 2DP doping efforts have focused on *p*-type doping,[14] primarily using I_2 vapor as an oxidant,[5] a method which provides little control over the number of free carriers introduced into these materials.[15], [16] Here, we explore controlled *n*-doping using cobaltocene that is introduced in well-defined stoichiometric amounts and undergoes an exergonic redox process with semiconducting 2DPs (**Figure 1**). This controlled *n*-doping enables an unprecedented systematic investigation of 2DP electronic and magnetic properties at precise carrier densities.

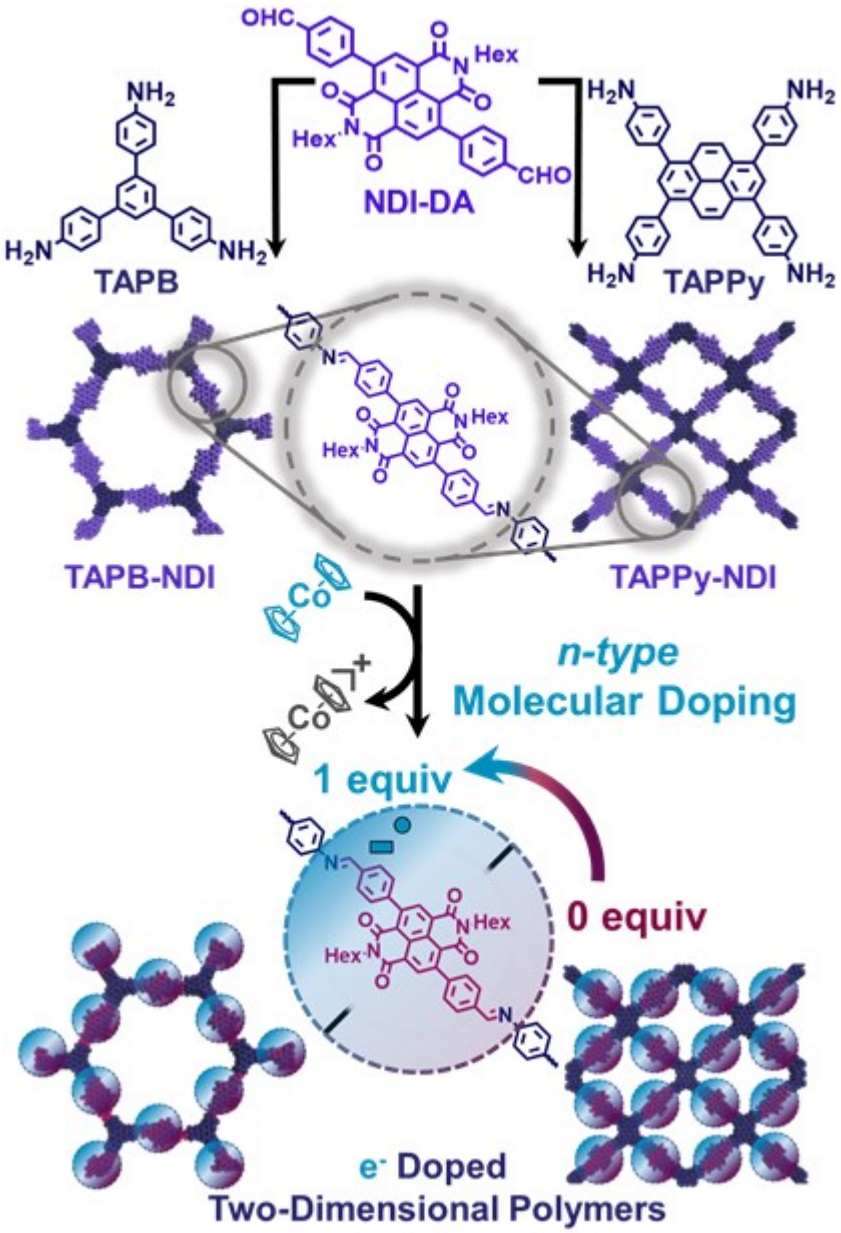

Figure 1. Synthesis of redox-active NDI-containing 2DPs followed by doping with defined stoichiometric amounts of molecular $CoCp_2$ (*n*-doping). The arrow from 0 to 1 equiv signifies the ability to systematically tune the amounts of NDI radical anions within the 2DP by changing the added amount of $CoCp_2$.

We synthesized two semiconducting 2DPs that contain naphthalene diimide (NDI) moieties and then *n*-doped them in defined stoichiometric amounts using cobaltocene ($CoCp_2$) (**Figure 1**). $CoCp_2$ is only capable of singly reducing NDI-species within the polymer to NDI-radical anions ($NDI^{\bullet-}$), thus producing paramagnetic *n*-doped 2DPs. One critical feature is that both 2DPs retain their crystallinity after doping, thus yielding structurally defined, organic semiconductors with well-controlled numbers of charge carriers. Maximum electronic conductivities of $>10^{-4}$ S cm^{-1} are observed at

substoichiometric doping levels.[17] Although π-bridges were incorporated between adjacent NDI units to promote in-plane coupling, in keeping with the prevalent design paradigm for electronically active 2DPs to-date, computational and experimental studies suggest that electronic coupling is stronger, and thus electronic conductivity is larger, in the inter-plane π-stacking direction.[18] These conductivities are observed despite appreciable in-plane conjugation, which has been the prevalent design focus for electronically active 2DPs to-date. Taken together, controlled molecular doping is shown to be a powerful strategy to access paramagnetic 2DP semiconductors, which are of interest for organic electronic and spintronic devices.

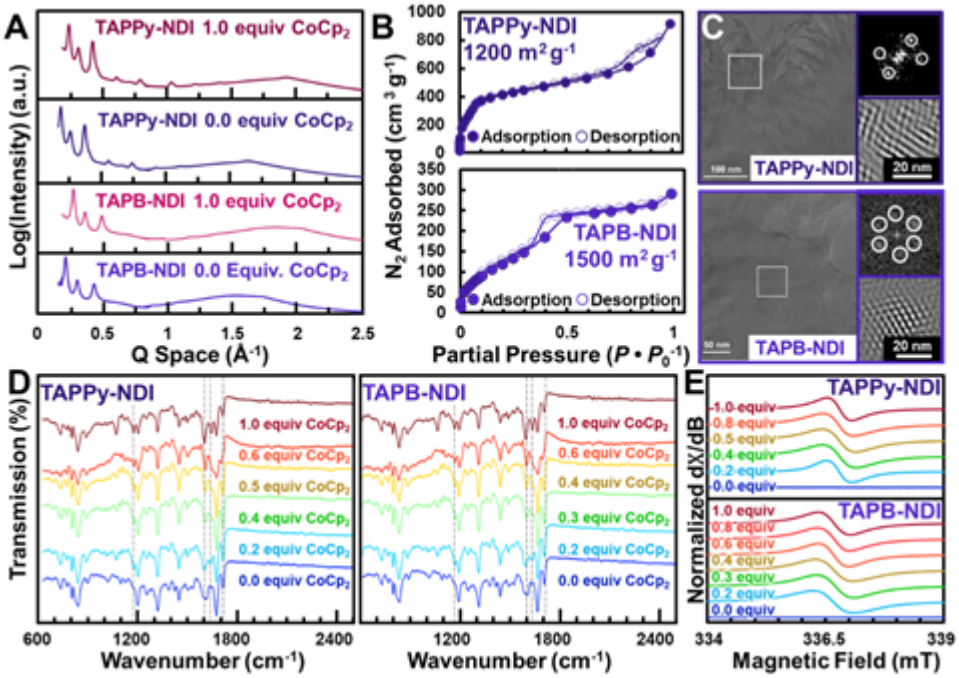

Figure 2. Chemical and structural characterization of undoped and *n*-doped 2DPs**. A)** Synchrotron X-ray diffraction of both as-synthesized undoped and fully doped (1 equiv $CoCp_2$ per NDI) NDI-based 2DPs. **B)** N_2 sorption isotherms for TAPPy-NDI (top) and TAPB-NDI (bottom). **C)** High-resolution transmission electron micrograph of TAPPy-NDI (top) and TAPB-NDI (bottom) with a Fourier-transform of a particular region (white box insets in Figure 2C, top right) and a band-pass filtered image of that region (bottom right). **D)** Fourier-transform infrared spectra of 2DPs variably doped with $CoCp_2$. **E)** Continuous-wave electron paramagnetic resonance spectra of pristine and variably doped NDI-based 2DPs.

NDI was chosen as the electron acceptor for our studies because its well-defined reduction potentials are accessible by many molecular reductants, as well as being suitable for many organic

semiconductor applications, leading to its extensive exploration in devices.[19] We have recently reported two-imine linked 2DPs based on a 3,7-di(4-formylphenyl)-functionalized NDI (NDI-DA) with different topologies; the condensation product of NDI-DA with 1,3,6,8-tetrakis(4-aminophenyl)pyrene (TAPPy, **Error! Reference source not found.**) under acetic acid-catalyzed conditions has a tetragonal lattice – TAPPy-NDI – and was reported as an example in a study of synthesis and isolation methodology,[20] while the product of NDI-DA and 1,3,5-tris(4-aminophenyl)benzene (TAPB, **Error! Reference source not found.**) has a hexagonal lattice – TAPB-NDI –and was studied as a lithium-ion battery material.[21] Both of these NDI-containing materials are suitable for *n*-doping studies and were resynthesized as high-quality polycrystalline powders using slightly modified conditions (**Error! Reference source not found.** and **Error! Reference source not found.**). Synchrotron X-ray diffraction (XRD) patterns collected at 13.3 keV (0.93 Å) of both TAPB-NDI and TAPPy-NDI powders have many sharp higher-order diffraction features (**Figure 2A**). The Pawley refined unit cells of the expected hexagonal TAPB-NDI lattice and tetragonal TAPPy-NDI lattice were found to match well with the respective experimental powder diffraction patterns.[22] When finite grain size feature broadening of the powder X-ray diffraction was considered, the average in-plane crystallographic length of both 2DPs was determined to be approximately 100 nm, consistent with current reports of high-quality 2DP powders.[23] Both 2DPs exhibited type IV N_2 isotherms with negligible hysteresis and high surface areas, which are representative of high quality materials. Brunauer-Emmet-Teller surface area analysis performed on these isotherms yield surface areas of 1500 $m^2\ g^{-1}$ and 1200 $m^2\ g^{-1}$ for TAPB-NDI and TAPPy-NDI, respectively (**Figure 2B**). From these N_2 isotherms, sharp pore size distributions centered at 2.9 nm and 3.4 nm were extracted for TAPB-NDI and TAPPy-NDI, both of which are consistent with their Pawley refined pore-structures. Transmission electron microscopy (TEM) images of both 2DPs corroborate that these powders are isolated as crystalline sheets with lateral dimensions of 100 nm (**Figure 2C** and **Error! Reference source not found.**-**Error! Reference source not found.**). Two-dimensional Fourier-transforms and band-pass filtered images of the TEM images are used to determine that hexagonally and tetragonally symmetric networks are isolated for TAPB-NDI and TAPPy-NDI, respectively (**Figure 2C insets**). Following polymerization and isolation, Fourier-transform infrared (FT-IR) spectroscopy exposed the emergence of the expected imine stretching frequency at 1670 cm^{-1} (**Figure 2D**). The amine (3000 cm^{-1}) and aldehyde (1710 cm^{-1}) FT-IR signals were reduced upon polymerization, which is consistent with the formation of imine bonds (Error! Reference source not found. and **Error! Reference source not found.**).[24] These measurements unambiguously demonstrate that both TAPB-NDI and TAPPy-NDI are prepared as highly crystalline powders with minimal unreacted functionalities.

Cobaltocene ($CoCp_2$) was used to singly reduce the incorporated NDI units to introduce unpaired electrons into both networks. Redox potentials evaluated by cyclic voltammetry (**Figure S50**) reveal that NDI units within the 2DP have a redox potentials similar to molecular NDIs, which suggests that complete one electron reduction to the radical anion ($NDI^{\bullet-}$) by $CoCp_2$ (-1.3 V vs. $FeCp_2$)[25] is expected. Both 2DPs were *n*-doped by immersing a known amount of polycrystalline powder into $CoCp_2$ THF solutions for at least 16 h under a N_2 atmosphere (**Error! Reference source not found.**). The 2DPs were then recovered by filtration, rinsed with deoxygenated THF, and characterized, all under an inert atmosphere. After introducing controlled substoichiometric amounts of $CoCp_2$, we observe an immediate and pronounced darkening of both NDI-based 2DPs. As both 2DPs are doped with increasing amounts of $CoCp_2$, a feature at 1720 cm^{-1} disappears and a feature at 1620 cm^{-1} appears, both of which are consistent with reduction of NDI to $NDI^{\bullet-}$ (**Figure 2D** and **Error! Reference source not found.**). Double reduction NDI subunits to NDI^{2-} (-1.6 V vs. $FeCp_2$) by $CoCp_2$ is unexpected based on the redox potentials of molecular NDIs,[19, 25] which is consistent with cyclic voltammetry measurements of NDI-containing frameworks and the observation that infrared spectra of frameworks that had 2 equiv. of $CoCp_2$ added are indistinguishable from those to which 1 equiv of $CoCp_2$ are added.

Prior to doping with $CoCp_2$ both 2DPs give no signal when examined using continuous-wave electron paramagnetic resonance (CW-EPR) spectroscopy, as is expected for closed shell diamagnetic organic polymers. After doping both 2DPs with any amount of $CoCp_2$, a pronounced CW-EPR signal was observed. Simulation of the spectra with the Hamiltonian, $\hat{H} = g_{iso}\mu_B \boldsymbol{SH}$, yields values of 2.0042 ± 0.0001 for g_{iso}, for both TAPPY-NDI and TAPB-NDI. The simulation matches well with the experimental data and the g_{iso} tensors are consistent with NDI-centered radicals (**Figure 2E** and **Figures S41-47**). The semi-quantitative CW-EPR intensity of this feature is found to linearly increase with the quantity of $CoCp_2$ used until high doping levels, after which spin-spin interactions decrease the measured EPR intensity (**Figure S48** and **Figure S49**). Taken together, these results establish that NDIs within the 2DP can be singly reduced by exposure to controlled amounts of $CoCp_2$.

After complete reduction (1.0 equiv $CoCp_2$), the X-ray diffraction patterns of both 2DPs change only slightly (**Figure 2A**), which indicates that the lattice is not substantially perturbed by the presence of embedded $NDI^{\bullet-}$ radical anions or the $CoCp_2^+$ counterions, which are presumably located in the channels and along the periphery of 2DP crystallites. However, minor shifts of the in-plane diffraction feature (0.1 $Å^{-1}$< Q Space <0.5 $Å^{-1}$) to lower scattering vector and the out-of-plane diffraction feature (1.5 $Å^{-1}$< Q Space <2.5 $Å^{-1}$) to higher scattering vector are observed. This suggests

that to accommodate the charges, counterions, and changes in bond length produced upon doping, the lattice becomes slightly more planar with tighter interlayer packing. These results demonstrate that NDI-based 2DPs with variable numbers of electronic carriers and paramagnetic centers can be produced through exposure to $CoCp_2$.

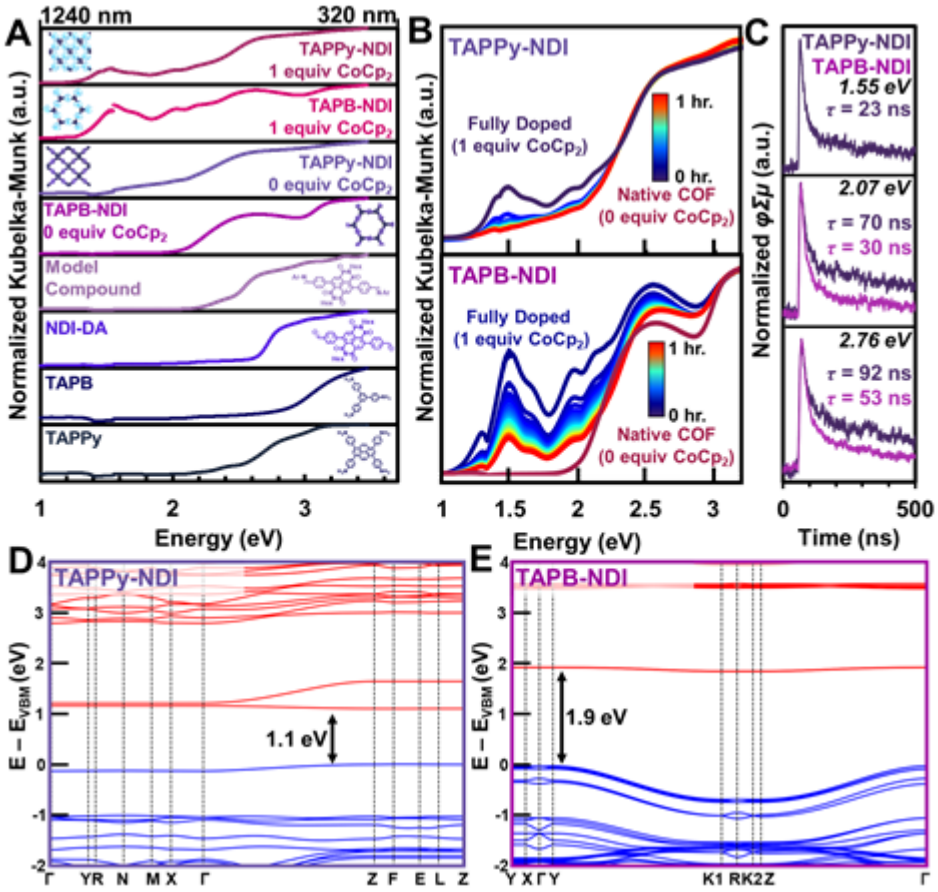

Figure 3. Optical characterization of monomers, model compounds, pristine 2DPs, and doped 2DPs and electronic structure of pristine 2DPs. A) Diffuse-reflectance ultraviolet-visible-near-IR spectroscopy of monomers, model compound, pristine NDI-containing 2DPs, and fully doped (1.0 equiv. $CoCp_2$ per NDI) NDI-containing 2DPs. The discontinuities in the spectra at 1.4 eV are due to a detector change-over within the instrument. **B)** Diffuse-reflectance ultraviolet-visible-near-IR spectroscopy during temporal evolution of fully doped NDI-containing 2DPs to entirely undoped upon exposure to air. **C)** Time-resolved flash-photolysis microwave conductivity of both pristine NDI-containing 2DPs and their charge-carrier lifetimes, inset text shows the excitation wavelength and the average amplitude-weighted lifetime, $\langle\tau\rangle$. **D)** Electronic band structures calculated at the PBE0 density functional theory level for pristine multilayer TAPPy-NDI and **E.** TAPB-NDI (valence bands in blue; conduction bands in red).

Both NDI-based 2DPs were found to have moderate energy optical transitions (<2 eV) in their undoped and doped states. Tauc analysis,[26] which is performed by extrapolating the linear region of absorbance to the abscissa, of diffuse-reflectance ultraviolet-visible (DR-UVVis) spectroscopy showed that powders of the NDI-DA, TAPB, and TAPPy monomers all have optical transitions above 2.25 eV, which likely originate from isolated molecular electronic transitions (and not infinitely delocalized electronic bands) (**Figure 3A** and **Figure S29**. By condensing NDI-DA with 4-*tert*-butylaniline, we determined that imine formation shifted the absorption edge of NDI-DA by 0.30 eV, consistent with both enhanced conjugation and charge-transfer behavior across an aromatic imine. However, 2D polymerization produced pronounced electronic shifts (>0.6 eV) to yield optical transitions of 1.8 eV and 1.3 eV for TAPB-NDI and TAPPy-NDI (**Figure 3A,** Error! Reference source not found.). The electronic structure of pristine TAPPy-NDI was also confirmed by ultraviolet and inverse photoelectron spectroscopy (UPS and IPES), which showed a single-particle gap of 1.57 eV for this material (**Error! Reference source not found.**). Electrostatic charging precluded this analysis for TAPB-NDI. These spectroscopic characterizations demonstrate that more electronically delocalized structures, likely in the cross-plane direction *vide infra*, are produced during polymerization of NDIs into a layered 2D polymer.

Flash-photolysis time-resolved microwave conductivity (fp-TRMC) measurements indicate that both 2DPs are intrinsically semiconducting and exhibit long-lived free charge carriers. By exciting undoped 2DPs with a laser pulse and then monitoring the 9GHz microwave absorption of photoinduced charge carriers, the product of charge carrier yield (φ) and the sum of their mobilities ($\Sigma\mu = \mu_{electron} + \mu_{hole}$) can be extracted (denoted as $\varphi\Sigma\mu$, **Error! Reference source not found.** and **Supporting Information Section J**). Additionally, by monitoring the transient microwave absorption, the lifetimes of photoinduced charge carriers can be extracted in a contactless manner. When excited at 2.76 eV (450 nm) and 2.07 eV (600 nm), TAPPy-NDI and TAPB-NDI both showed appreciable photoconductivity with $\varphi\Sigma\mu$ values of *ca.* 5×10^{-5} $cm^2V^{-1}s^{-1}$ (**Figure 3C**). When excited at 1.55 eV (800 nm), only the TAPPy-NDI exhibited a measurable photoconductivity ($\varphi\Sigma\mu$ of *ca.* 5×10^{-5} $cm^2V^{-1}s^{-1}$, **Error! Reference source not found.29**, **Figure S30**, and **Tables S2-S3**), consistent with the lower energy optical bandgap of TAPPy-NDI assessed by DR-UVVis. Global biexponential fp-TRMC transients for both 2DPs at all photon energies are characterized by a short time component (τ_1, *ca.* 4 - 12 ns) over which a large reduction in free carrier population occurs and a longer one (τ_2, *ca.* 290 - 400 ns) characteristic of the charges that remain. Compared to the global biexponential fit parameters for TAPB-NDI, TAPPy-NDI generally showed a slightly smaller τ_1 lifetime component (by

~40%) at 2.07 and 2.76 eV. In contrast, TAPPy-NDI's τ_2 was larger than TAPB-NDI's by ~100 ns at each photon energy (**Figure 3C** and **Error! Reference source not found.**). For both 2DPs, τ_1 and τ_2 decreased with decreasing photon energy with τ_1 generally becoming more heavily weighted; suggesting that the fast dynamics increasingly dominate our fp-TRMC transients with lower energy excitation (**Error! Reference source not found.**). Although various factors could explain the biexponential nature of these transients, the dynamics are consistent with sizeable trapping rate constants for either electrons or holes that quickly (≤12 ns) fill trap states with complementary longer-lived charge carriers (*ca.* 290 - 400 ns).[27] This is consistent with TEM images that reveal ill-defined 2DP particles indicative of structural defects that may introduce potential trap states. The photoconductivity of these NDI-based 2DPs is substantially different from its monomer species, highlighting how periodic arrays of chromophores can facilitate charge transport (See **Supporting Information Section J**). Overall, fp-TRMC measurements suggest that both NDI-based 2DPs are intrinsic semiconductors.

To gain insight into the electronic structure of the NDI-containing 2DPs, we performed electronic-structure calculations using density functional theory (DFT) (see **Supporting Information Section K** for the details of the DFT computational methodology). Briefly, the bulk crystal structures were optimized at the PBE level with the D3 van der Waals (vdW) dispersion corrections (**Error! Reference source not found.**); the band structures were then calculated using the PBE0 functional. The conduction band edges of both 2DPs (**Figure 3D** and **3E**) are dispersionless along the in-plane directions owing to poor in-plane conjugation from the large dihedral angles between the NDI moieties and the TAPPy or TAPB moieties. Along the out-of-plane directions (Γ-Z), there appears a weak dispersion in the lowest conduction band, 0.05 and 0.07 eV for TAPPy-NDI and TAPB-NDI, respectively, which is indicative of a weak electronic coupling among NDI fragments due to π-π stacking. This small dispersion implies that both NDI 2DPs are expected to exhibit hopping-type transport between localized redox sites in the out-of-plane direction. The calculations point to direct bandgaps ($E_{CB} - E_{VB}$) of 1.1 eV and 1.9 eV for TAPPy-NDI (**Figure 3D**) and TAPB-NDI (**Figure 3E**), respectively, both of which are qualitatively consistent with the optical absorption and fp-TRMC measurements. [28] To further characterize the inter-layer *vs*. intra-layer effects on the 2DP electronic structure, we also calculated the electronic band structure for monolayers of TAPB-NDI and TAPPy-NDI (**Error! Reference source not found.**-**Error! Reference source not found.**). In the absence of multilayer stacking, the bottom conduction (and top valence) bands are entirely flat and larger band gaps are obtained, which confirms that the intra-layer coupling among NDI units is vanishingly small. Therefore, ordered interlayer stacking is necessary to achieve significant electronic conductivities in these NDI-based 2DPs. In order to describe the nature of the optical gaps in the two NDI-based 2DPs,

we analyzed the projected densities of states (PDOS) and simulated the optical absorption spectra (**Error! Reference source not found.**). The weak and broad absorption peaks in both 2DPs display a charge-transfer character, associated with a transition from the top valence bands, dominated by contributions from the TAPPy/TAPB cores, to the bottom conduction bands, dominated by contributions from the NDI linkers.

When fully doped (1.0 equiv $CoCp_2$ per NDI) TAPB-NDI and TAPPy-NDI exhibit the emergence of 1.25 eV and 1.15 eV optical transitions, respectively, both of which are consistent with the presence of $NDI^{\bullet-}$ subunits observed by electron paramagnetic resonance spectroscopy.[29],[30] When exposed to air, $NDI^{\bullet-}$ is known to oxidize back to its native state (NDI),[19] which we observed over the course of one hour for $NDI^{\bullet-}$-containing frameworks using FT-IR spectroscopy (Error! Reference source not found.-Error! Reference source not found.). Therefore, continually collecting DR-UVVis spectra of a fully doped 2DP sample while the sample is exposed to air allows us to examine many intermediate doped states within a single experiment. As both 2DPs are exposed to air, we find that the optical absorption features associated with the $NDI^{\bullet-}$ state gradually decrease. Similarly, the FT-IR spectra and XRD patterns of doped NDI-containing 2DPs following oxidation are indistinguishable from those of the pristine material. These findings suggest that $NDI^{\bullet-}$-containing 2DPs have low energy optical transitions and can be chemically reduced and then re-oxidized without significant chemical or structural degradation. The combination of theoretical calculations and static- and transient-optical spectroscopies motivated us to interrogate the bulk electronic conductivity of *n*-doped 2DP semiconductors.

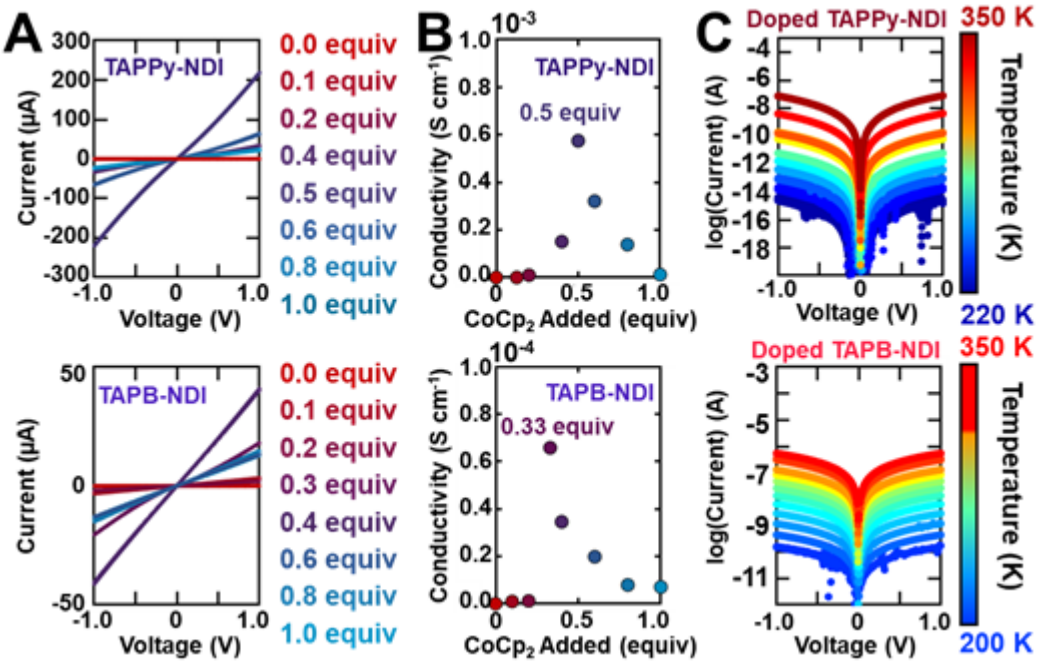

Figure 4. Conductivity measurements of controllably doped NDI-containing 2DPs. **A)** Current-voltage measurements of variably doped TAPPy-NDI (top) and TAPB-NDI (bottom) and **B)** extracted conductivities from **A**. **C)** Temperature-dependent conductivity of TAPPy-NDI (0.5 equiv $CoCp_2$, top) and of TAPB-NDI (1.0 equiv $CoCp_2$, bottom).

Two-probe pressed pellet conductivity measurements show that both 2DPs become several orders-of-magnitude more conductive upon doping. To measure the room-temperature bulk electronic conductivity of NDI-based 2DPs, powders were gently pressed between two copper rods in a nitrogen atmosphere and current was measured as a function of applied bias, with several voltage sweeps in both polarization directions (**Figure 4A** and **Error! Reference source not found.**). In all cases, no hysteresis was observed, which led us to treat these pressed pellets as idealized Ohmic resistors (**Error! Reference source not found.**). From this analysis, undoped TAPB-NDI and TAPPy-NDI are both found to be insulating with conductivities of $<10^{-9}$ S cm^{-1}, which is consistent with expectations of chemically pure intrinsic semiconductors with greater than 1 eV bandgaps at room temperature (**Figure 4A-B**). The electronic conductivities gradually increased to a maximum of 6×10^{-4} S cm^{-1} for TAPPy-NDI and 7×10^{-5} S cm^{-1} for TAPB-NDI as charge-carriers are contributed by chemical reduction (**Figure 4A-B**). This order-of-magnitude difference in conductivity is qualitatively consistent with DFT calculation and spectroscopic measurements that show more delocalized character and longer lived charge-carriers, consistent with larger relative carrier mobilities, in TAPPy-NDI. In both cases, maximum conductivity is observed at substoichiometric cobaltocene doping, with TAPB-NDI having an optimal doping of 0.33 equiv $CoCp_2$ and TAPPy-NDI having an optimal doping of

0.50 equiv $CoCp_2$, which likely reflects a balancing of charge carrier density and open hopping sites that is commonly observed in semiconducting polymers. This finding highlights another advantage of controlled stoichiometric doping, for which optimal charge carrier concentrations can be reliably targeted.

Variable-temperature conductivity experiments indicate a thermally activated process. As the temperature is decreased by 100 K, the electronic conductivity of both doped 2DPs decreases over 5 orders-of-magnitude (**Figure 4C**) following an Arrhenius relationship with temperature (**Error! Reference source not found.**, again consistent with a hopping mechanism, which is frequently observed when redox-active sites within weakly dispersive bands are held in close proximity, such as the van der Waals contact in the macromolecular sheets studied here.[18] However, more mechanistic analysis is necessary to definitively determine the charge-transport pathways that lead to the temperature-enhanced electronic conductivities observed here.

The maximum conductivities demonstrated at these substoichiometric doping levels are comparable with those obtained in many studies of doped linear NDI polymers, although falling short of the highest values reported for NDI-containing polymers.[31] However, they are substantially lower than the highest conductivity values reported for the most developed *p*- (>10^4 S cm^{-1})[12, 32] and *n*-doped (>90 S cm^{-1})[33], [34] organic materials. The low density of electronically active NDI-sites, their weak electronic couplings, and the substantial porosity of the 2DPs reported here explain, at least in part, this difference in electronic conductivity. However, there exists substantial design potential to enhance the subunit electronic coupling either in-plane or out-of-plane, both of which would increase the bulk electronic conductivity of 2DPs. Specifically, this report demonstrates that moderate electronic conductivities, comparable to those in similar linear polymers, can be realized by intimate van der Waals contact, which can likely be systematically engineered in macromolecular sheets. Finally, the isotropic bulk conductivities reported here are likely diminished by the pressed pellet sample geometry, which are limited by the least conductive crystallographic direction and are significantly deteriorated due to interfacial resistance at the electrodes and particle boundaries. Therefore, it is conceivable that intrinsic intracrystallite transport may be significantly higher than the bulk values observed here. To address these limitations, future studies should aim to improve 2DP molecular design and better control 2DP morphology (*e.g.* synthesis as highly crystalline and oriented thin films), both of which are expected to enhance bulk conductivities.

This report demonstrates that paramagnetic, semiconducting 2DPs with meaningful electronic transport can be accessed by controlled molecular doping. More importantly, this approach enables the systematic investigation of paramagnetic and electronic behavior in covalently linked crystalline

organic systems at controlled carrier densities, which is critical for the advancement of electronic 2DP design. As such, controlled molecular doping of 2DPs is a promising strategy that will undoubtedly inspire future investigations of other chemically and topologically distinct redox-active 2DPs and their associated electronic and spintronic devices.

Methods

General 2DP doping procedure: polycrystalline powders (typically 25-50 mg) were preweighed into prelabeled vials under a N_2 atmosphere. Then, separately, a $CoCp_2$ solution was prepared at a known concentration in anhydrous THF (See **Error! Reference source not found.** below for representative calculation details). Then, a volume of this molecular dopant solution was added to the powders in amounts to target the desired doping ratio. Nearly immediately the undoped powders were found to transform from a light yellow orange to a dark burgundy. 2DP powders then sat undisturbed within the dopant solution for at least 16 h. These solutions were then filtered and rinsed extensively (50 mL) with clean solvent THF.

Synchrotron X-ray Diffraction. Synchrotron powder X-ray diffraction was collected at either Sector 5 or 12 of the Advanced Photon Source, Argonne National Lab. All two-dimensional frames were collected in a transmission geometry then summed and radially integrated to produce a linear PXRD pattern using proprietary software available at the APS. The sample-to-detector distance was adjusted to measure across relevant detection ranges of q. Scattering intensity is reported as a function of the modulus of the scattering vector Q, related to the scattering angle 2θ by the equation $Q = (4\pi/\lambda) \sin \theta$, where λ is the x-ray wavelength.

Two-probe pressed pellet measurements: Powders were loaded into a hollowed glass rod. The powders were finger tightened between the rods and the two copper bars were then equipped to a potentiostat. We ran several potential sweeps in both bias directions to check for hysteretic behavior. In all cases, we observed no hysteresis, which led us to consider these materials as idealized Ohmic resistors. At the end of the experiment, we measured the length of the pressed pellet using dial calipers by measuring the difference of the full assembly with and without the powders. This distance, with the obtained IV curves, was used to evaluate the Ohmic resistance.

Electron paramagnetic resonance measurements: Continuous wave electron paramagnetic resonance (CW-EPR) spectra were acquired using a Bruker ELEXYS E500 spectrometer operating at X-band (9.4 GHz) frequencies with an Oxford ESR900 He flow cryostat with an ITC-5025 temperature controller and a Bruker High QE (HQE) cavity resonator (ER 4122SHQE).

Supporting Information

Supporting Information is available from the Wiley Online Library or the author.

Acknowledgements

We thank the Army Research Office for a Multidisciplinary University Research Initiatives (MURI) award under grant W911NF-15-1-0447, which supported the preparation of electroactive 2DPs, their optical characterization, and their study using density functional theory. We also thank the Department of Energy grant DE-SC0019356 for supporting efforts at controlled molecular doping, including the investigation of charge transport, electronic structure, and paramagnetic behavior. A.M.E. (DGE-1324585), K.A.C. (DGE-1842165), I.C. (DGE-11842165), M.J.S (DGE-11842165) are supported by the National Science Foundation Graduate Research Fellowship. S.J. thanks the United States-India Educational Foundation (USIEF, India) and the Institute of International Education (IIE, USA) for a Fulbright-Nehru Postdoctoral Fellowship (grant no. 2266/FNPDR/2017). Work in Princeton was supported in part by a grant of the National Science Foundation (DMR-1807797) (H.L.S and A.K.) and by a National Science Foundation Graduate Research Fellowship (DGE-1656466) (H.L.S.). This study made use of the IMSERC and EPIC at Northwestern University, both of which have received support from the Soft and Hybrid Nanotechnology Experimental (SHyNE) Resource (NSF NNCI-1542205 and NSF ECCS1542205, respectively), the Materials Research Science and Engineering Center (NSF DMR-1720139), the State of Illinois, and the International Institute for Nanotechnology (IIN). Portions of this work were performed at the DuPont-Northwestern-Dow Collaborative Access Team (DND-CAT) located at Sector 5 and Sector 8 of the Advanced Photon Source (APS). DND-CAT is supported by Northwestern University, E.I. DuPont de Nemours & Co., and the Dow Chemical Company. This research used resources of the Advanced Photon Source and Center for Nanoscale Materials, both U.S. Department of Energy (DOE) Office of Science User Facilities operated for the DOE Office of Science by Argonne National Laboratory under contract DE-AC02-06CH11357, and the National Energy Research Scientific Computing Center, a DOE Office of Science User Facility supported by the Office of Science of the U.S. Department of Energy under Contract No. DE-AC02-05CH11231. Resources at the Advanced Photon Source were funded by NSF under award 0960140. This work was authored by the National Renewable Energy Laboratory, operated by Alliance for Sustainable Energy, LLC, for the U.S. Department of Energy (DOE) under Contract No. DE-AC36-08GO28308. Funding for microwave measurements was provided by Department of Energy, Office of Basic Energy Sciences, Division of Chemical Sciences, Biosciences, and Geosciences. The views expressed in the article do not necessarily represent the views of the DOE or the U.S. Government. The U.S. Government retains and the publisher, by accepting the article for publication, acknowledges that the U.S. Government retains a nonexclusive, paid-up, irrevocable, worldwide license to publish or reproduce the published form of this work, or allow others to do so, for U.S.

Government purposes. T.G.A and G.R. thank Obadiah Reid for helpful discussions regarding microwave measurements.

Conflict of Interest

The authors declare no competing interests.

References

[1] K. Geng, T. He, R. Liu, S. Dalapati, K. T. Tan, Z. Li, S. Tao, Y. Gong, Q. Jiang, D. Jiang, *Chem. Rev.* **2020**, *120*, 8814.
[2] Y. Yusran, Q. Fang, V. Valtchev, *Adv. Mater.* **2020**, 2002038; A. P. Cote, A. I. Benin, N. W. Ockwig, M. O'Keeffe, A. J. Matzger, O. M. Yaghi, *Science* **2005**, *310*, 1166.
[3] M. Dogru, T. Bein, *Chem. Comm.* **2014**, *50*, 5531.
[4] S. Jin, X. Ding, X. Feng, M. Supur, K. Furukawa, S. Takahashi, M. Addicoat, M. E. El-Khouly, T. Nakamura, S. Irle, S. Fukuzumi, A. Nagai, D. Jiang, *Angew. Chem. Int. Ed.* **2013**, *125*, 2071; X. Ding, L. Chen, Y. Honsho, X. Feng, O. Saengsawang, J. Guo, A. Saeki, S. Seki, S. Irle, S. Nagase, V. Parasuk, D. Jiang, *J. Am. Chem. Soc.* **2011**, *133*, 14510; D. D. Medina, M. L. Petrus, A. N. Jumabekov, J. T. Margraf, S. Weinberger, J. M. Rotter, T. Clark, T. Bein, *ACS Nano* **2017**, *11*, 2706; N. Keller, D. Bessinger, S. Reuter, M. Calik, L. Ascherl, F. C. Hanusch, F. Auras, T. Bein, *J. Am. Chem. Soc.* **2017**, *139*, 8194; B. Sun, C.-H. Zhu, Y. Liu, C. Wang, L.-J. Wan, D. Wang, *Chem. Mater.* **2017**, *29*, 4367; T. Sick, A. G. Hufnagel, J. Kampmann, I. Kondofersky, M. Calik, J. M. Rotter, A. Evans, M. Döblinger, S. Herbert, K. Peters, D. Böhm, P. Knochel, D. D. Medina, D. Fattakhova-Rohlfing, T. Bein, *J. Am. Chem. Soc.* **2017**, *140*, 2085; M. Dogru, M. Handloser, F. Auras, T. Kunz, D. Medina, A. Hartschuh, P. Knochel, T. Bein, *Angew. Chem. Int. Ed.* **2013**, *125*, 2992; D. Bessinger, L. Ascherl, F. Auras, T. Bein, *J. Am. Chem. Soc.* **2017**, *139*, 12035; G. H. Bertrand, V. K. Michaelis, T.-C. Ong, R. G. Griffin, M. Dincă, *Proc. Nat. Acad. Sci.* **2013**, *110*, 4923; T. Li, W.-D. Zhang, Y. Liu, Y. Li, C. Cheng, H. Zhu, X. Yan, Z. Li, Z.-G. Gu, *J. Mat. Chem. A* **2019**, *7*, 19676.
[5] S. Wan, J. Guo, J. Kim, H. Ihee, D. Jiang, *Angew. Chem. Int. Ed.* **2009**, *48*, 5439; E. Jin, M. Asada, Q. Xu, S. Dalapati, M. A. Addicoat, M. A. Brady, H. Xu, T. Nakamura, T. Heine, Q. Chen, D. Jiang, *Science* **2017**, *357*, 673; V. Lakshmi, C.-H. Liu, M. Rajeswara Rao, Y. Chen, Y. Fang, A. Dadvand, E. Hamzehpoor, Y. Sakai-Otsuka, R. S. Stein, D. F. Perepichka, *J. Am. Chem. Soc.* **2020**, *142*, 2155.
[6] S. Jhulki, A. M. Evans, X.-L. Hao, M. W. Cooper, C. H. Feriante, J. Leisen, H. Li, D. Lam, M. C. Hersam, S. Barlow, W. R. Dichtel, S. R. Marder, *J. Am. Chem. Soc.* **2020**, *142*, 783; A. M. Evans, N. P. Bradshaw, B. Litchfield, M. J. Strauss, B. Seckman, M. R. Ryder, I. Castano, C. Gilmore, N. C. Gianneschi, C. R. Mulzer, M. C. Hersam, W. R. Dichtel, *Adv. Mater.* **2020**, *32*, 2004205; L. Ascherl, E. W. Evans, J. Gorman, S. Orsborne, D. Bessinger, T. Bein, R. H. Friend, F. Auras, *J. Am. Chem. Soc.* **2019**, *141*, 15693.
[7] S. Fratini, M. Nikolka, A. Salleo, G. Schweicher, H. Sirringhaus, *Nat. Mater.* **2020**; B. Lussem, C.-M. Keum, D. Kasemann, B. Naab, Z. Bao, K. Leo, *Chem. Rev.* **2016**, *116*, 13714.
[8] J. Devkota, R. Geng, R. C. Subedi, T. D. Nguyen, *Adv. Func. Mater.* **2016**, *26*, 3881.
[9] B. Russ, A. Glaudell, J. J. Urban, M. L. Chabinyc, R. A. Segalman, *Nat. Rev. Mater.* **2016**, *1*, 1.
[10] K. Walzer, B. Maennig, M. Pfeiffer, K. Leo, *Chem. Rev.* **2007**, *107*, 1233; S. Barlow, S. R. Marder, X. Lin, F. Zhang, A. Kahn, in *Conjugated Polymers: Properties, Processing, and Applications*, 2019.

[11] I. E. Jacobs, A. J. Moulé, *Adv. Mater.* **2017**, *29*, 1703063; I. Salzmann, G. Heimel, M. Oehzelt, S. Winkler, N. Koch, *Acc. Chem Res.* **2016**, *49*, 370.
[12] Y. Yamashita, J. Tsurumi, M. Ohno, R. Fujimoto, S. Kumagai, T. Kurosawa, T. Okamoto, J. Takeya, S. Watanabe, *Nature* **2019**, *572*, 634.
[13] H. Li, H. Li, S. Xun, J.-L. Brédas, *Chem. Mater.* **2020**, *32*, 9228.
[14] J. M. Rotter, R. Guntermann, M. Auth, A. Mähringer, A. Sperlich, V. Dyakonov, D. D. Medina, T. Bein, *Chem. Sci.* **2020**, *11*, 12843.
[15] Q. Zhang, M. Dai, H. Shao, Z. Tian, Y. Lin, L. Chen, X. C. Zeng, *ACS Appl. Mater. Interfaces* **2018**, *10*, 43595.
[16] I_2 is a not an ideal dopant because it is challenging to introduce in controlled amounts, has an oxidation potential not well-matched with most aromatic systems, is volatile and desorbs over time, and produces an I_3^- counterion that is itself electronically conductive. These factors complicate understanding of the electronic properties of 2DPs doped with iodine.
[17] J. Petersen, C. Schramm, D. Stojakovic, B. M. Hoffman, T. J. Marks, *J. Am. Chem. Soc.* **1977**, *99*, 286.
[18] L. S. Xie, G. Skorupskii, M. Dincă, *Chem. Rev.* **2020**.
[19] M. Al Kobaisi, S. V. Bhosale, K. Latham, A. M. Raynor, S. V. Bhosale, *Chem. Rev.* **2016**, *116*, 11685.
[20] C. H. Feriante, S. Jhulki, A. M. Evans, R. R. Dasari, K. Slicker, W. R. Dichtel, S. R. Marder, *Adv. Mater.* **2020**, *32*, 1905776.
[21] S. Jhulki, C. H. Feriante, R. Mysyk, A. M. Evans, A. Magasinski, A. S. Raman, K. Turcheniuk, S. Barlow, W. R. Dichtel, G. Yushin, S. R. Marder, *ACS Appl. Energy Mater.* **2020**.
[22] G. Pawley, *J. Appl. Crystallogr.* **1981**, *14*, 357.
[23] M. C. Daugherty, E. Vitaku, R. L. Li, A. M. Evans, A. D. Chavez, W. R. Dichtel, *Chem. Commun.* **2019**, *55*, 2680.
[24] Although the signal at 1710 cm–1, corresponding to the aldehyde C=O stretching mode, does not completely disappear, this is attributable to overlap with a carbonyl stretching mode of the NDI core
[25] N. G. Connelly, W. E. Geiger, *Chem. Rev.* **1996**, *96*, 877.
[26] T. Sick, A. G. Hufnagel, J. Kampmann, I. Kondofersky, M. Calik, J. M. Rotter, A. Evans, M. Doeblinger, S. Herbert, K. Peters, D. Boehm, P. Knochel, D. D. Medina, D. Fattakhova-Rohlfing, T. Bein, *J. Am. Chem. Soc.* **2018**, *140*, 2085.
[27] A. C. Jakowetz, T. F. Hinrichsen, L. Ascherl, T. Sick, M. Calik, F. Auras, D. D. Medina, R. H. Friend, A. Rao, T. Bein, *J. Am. Chem. Soc.* **2019**, *141*, 11565.
[28] V. Coropceanu, J. Cornil, D. A. da Silva Filho, Y. Olivier, R. Silbey, J.-L. Brédas, *Chem. Rev.* **2007**, *107*, 926.
[29] Cobaltecinium is weakly absorbing in the visible, with a peak at 405 nm and an extinction coefficient of only 200 M^-1 cm^-1. This highlights an advantage of CoCp2 for systematic studies of controlled doping in NDI systems.
[30] G. Andric, J. F. Boas, A. M. Bond, G. D. Fallon, K. P. Ghiggino, C. F. Hogan, J. A. Hutchison, M. A.-P. Lee, S. J. Langford, J. R. Pilbrow, *Aust. J. Chem.* **2004**, *57*, 1011.
[31] J. Liu, L. Qiu, R. Alessandri, X. Qiu, G. Portale, J. Dong, W. Talsma, G. Ye, A. A. Sengrian, P. C. Souza, *Adv. Mater.* **2018**, *30*, 1704630.
[32] K. Kang, S. Watanabe, K. Broch, A. Sepe, A. Brown, I. Nasrallah, M. Nikolka, Z. Fei, M. Heeney, D. Matsumoto, *Nat. Mater.* **2016**, *15*, 896; V. Vijayakumar, Y. Zhong, V. Untilova, M. Bahri, L. Herrmann, L. Biniek, N. Leclerc, M. Brinkmann, *Adv. Energy Mater.* **2019**, *9*, 1900266.
[33] Y. Lu, J.-Y. Wang, J. Pei, *Chem. Mater.* **2019**, *31*, 6412.
[34] Y. Lu, Z. D. Yu, H. I. Un, Z. F. Yao, H. Y. You, W. Jin, L. Li, Z. Y. Wang, B. W. Dong, S. Barlow, S. R. Marder, J. Pei, **2021**, *33*, 2005946.

Figures and Captions

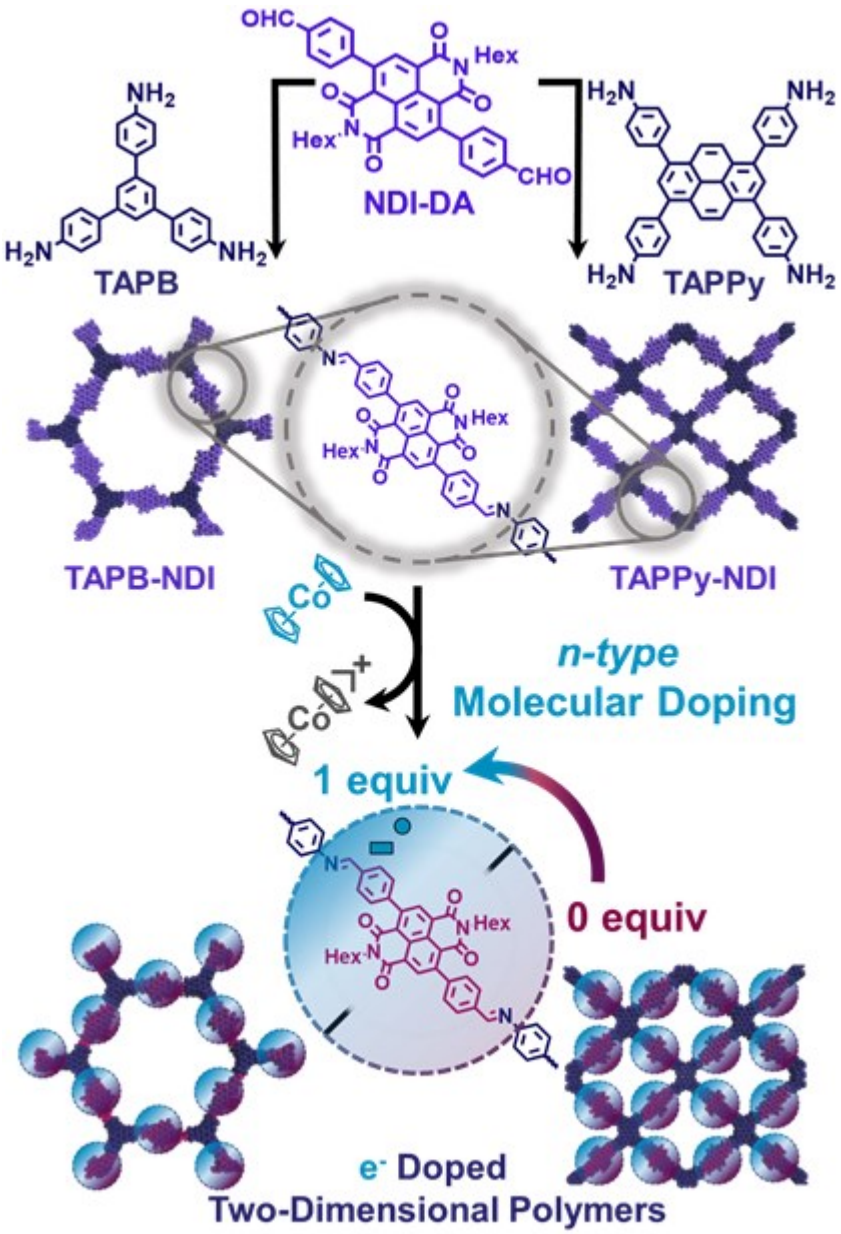

Figure 1. Synthesis of redox-active NDI-containing 2DPs followed by doping with defined stoichiometric amounts of molecular $CoCp_2$ (*n*-doping). The arrow from 0 to 1 equiv signifies the ability to systematically tune the amounts of NDI radical anions within the 2DP by amount of $CoCp_2$ added.

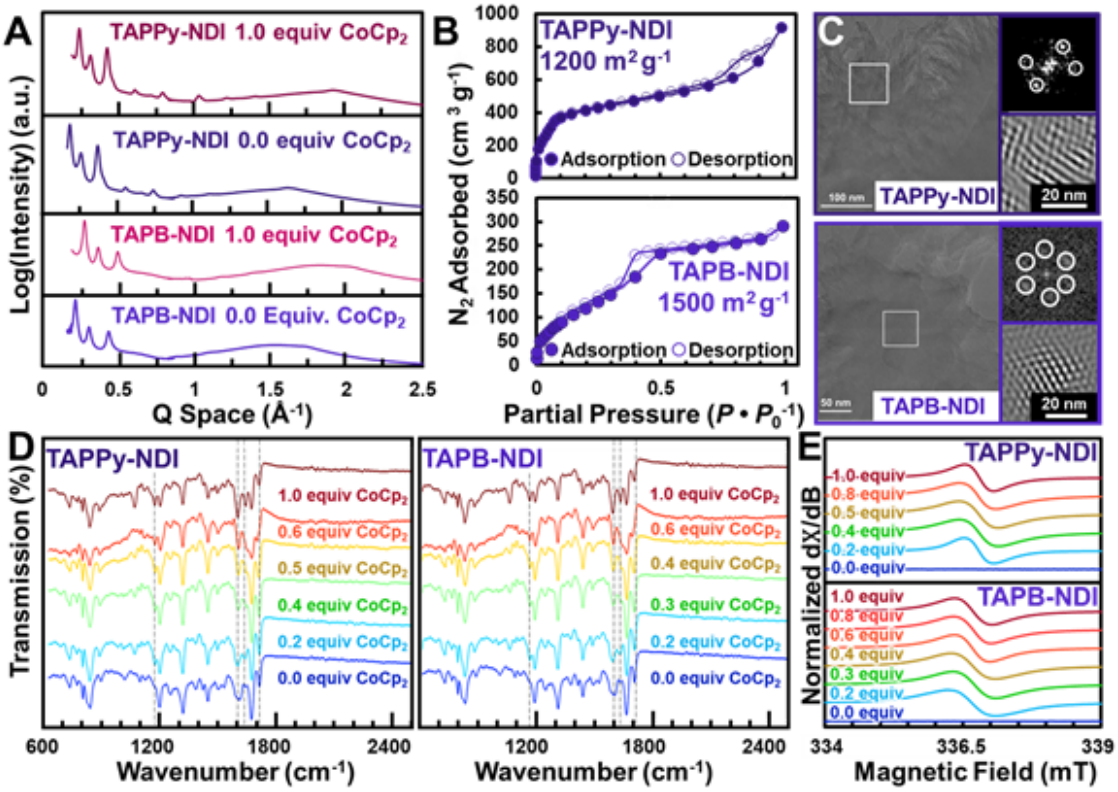

Figure 2. Chemical and structural characterization of undoped and *n*-doped 2DPs**. A)** Synchrotron X-ray diffraction of both as-synthesized undoped and fully doped (1 equiv $CoCp_2$ per NDI) NDI-based 2DPs. **B)** N_2 sorption isotherms for TAPPy-NDI (top) and TAPB-NDI (bottom). **C)** High-resolution transmission electron micrograph of TAPPy-NDI (top) and TAPB-NDI (bottom) with a Fourier-transform of a particular region (white box in Figure 2C, top right) and a band-pass filtered image of that region (bottom right).**D)** Fourier-transform infrared spectra of 2DPs variably doped with $CoCp_2$. **E)** Continuous-wave electron paramagnetic resonance spectra of pristine and variably doped NDI-based 2DPs.

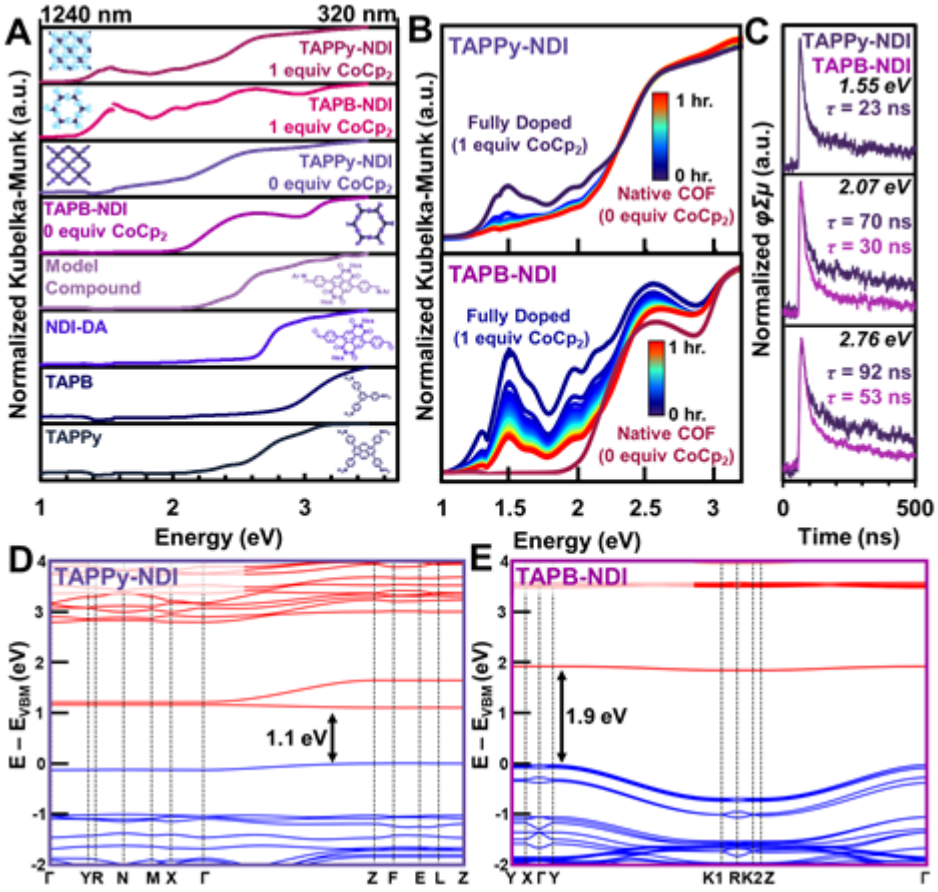

Figure 3. Optical characterization of monomers, model compounds, pristine 2DPs, and doped 2DPs and electronic structure of pristine 2DPs. **A)** Diffuse-reflectance ultraviolet-visible-near-IR spectroscopy of monomers, model compound, pristine NDI-containing 2DPs, and fully doped (1.0 equiv. $CoCp_2$ per NDI) NDI-containing 2DPs. The discontinuities in the spectra ~1.4 eV are due to a detector change-over within the instrument. **B)** Diffuse-reflectance ultraviolet-visible-near-IR spectroscopy during temporal evolution of fully doped NDI-containing 2DPs to entirely undoped upon exposure to air. **C)** Time-resolved flash-photolysis microwave conductivity of both pristine NDI-containing 2DPs and their charge-carrier lifetimes, inset text shows the excitation wavelength and the amplitude-weighted lifetime, $\langle\tau\rangle$. **D)** Electronic band structures calculated at the PBE0 density functional theory level for pristine multilayer TAPPy-NDI and E. TAPB-NDI (valence bands in blue; conduction bands in red).

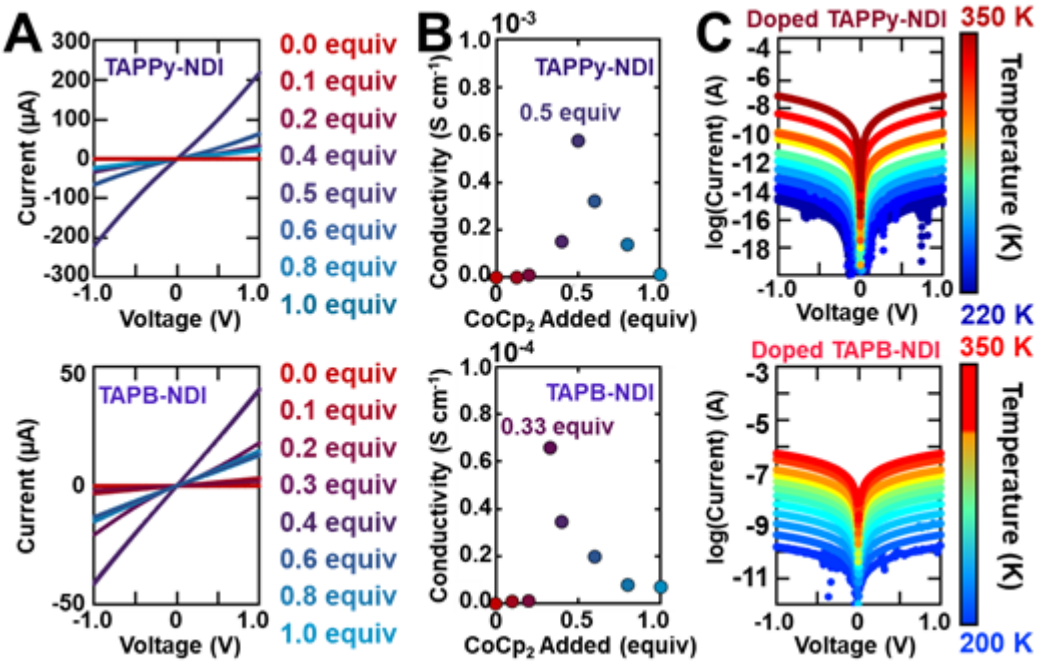

Figure 4. Conductivity measurements of controllably doped NDI-containing 2DPs. **A)** Current-voltage measurements of variably doped TAPPy-NDI (top) and TAPB-NDI (bottom) and **B)** extracted conductivities from **A**. **C)** Temperature-dependent conductivity of TAPPy-NDI (0.5 equiv $CoCp_2$, top) and of TAPB-NDI (1.0 equiv $CoCp_2$, bottom).

Table of Contents

TOC Text: The bulk conductivity of naphthalene diimide-based two-dimensional polymers is increased by controlled stoichiometric *n*-doping with cobaltocene. Following single-electron reduction, these 2DPs retain their periodic structure and become paramagnetic. Substoichiometric doping leads to the highest bulk electronic conductivities, which is found to proceed through a hopping-mechanism.

Keywords: Two-dimensional polymers, controlled *n*-doping, organic semiconductors

Primary Keyword: Two-dimensional polymer doping

Austin M. Evans, Kelsey A. Collins, Sangni Xun, Taylor G. Allen, Samik Jhulki, Ioannina Castano, Hannah L. Smith, Michael J. Strauss, Alexander K. Oanta, Lujia Liu, Lei Sun, Obadiah G. Reid, Gjergji Sini, Danilo Puggioni, James M. Rondinelli, Tijana Rajh, Nathan C. Gianneschi, Antoine Kahn, Danna E. Freedman, Hong Li, Stephen Barlow, Garry Rumbles', Jean-Luc Brédas, Seth R. Marder, William R. Dichtel*

Controlled *n*-Doping of Naphthalene Diimide-Based Two-Dimensional Polymers